

Vortical Flow Behind Isolated Helicopter Fuselage

Andrey S. Batrakov[†], Alexander N. Kusyumov[†], Sergey A. Mikhailov[†], Lyaisan I. Garipova[†] and George N. Barakos[‡]

[†]Tupolev Kazan National Research Technical University
10 Karl Marx St., Kazan 420111, Russian Federation
Email: postbox7@mail.ru,

[‡]School of Engineers, University of Liverpool
Liverpool, L69 3GH, U.K.
Email: G.Barakos@liverpool.ac.uk

ABSTRACT

This paper presents a Computational Fluid Dynamics study of the flow structures behind a helicopter fuselage. Helicopters, in general, are not as streamlined as fixed-wing aircraft and their fuselages may have large areas of flow stagnation as well as rear-facing surfaces with suction and flow separation. Further complications with this flow arise from the possibility of the flow to be unsteady if the separation region becomes large. After validation against experiments, the Computational Fluid Dynamics results are used to study the structure and flow topology behind a realistic helicopter fuselage. It is evident that relatively small details of the geometry can have significant effect on the flow structures and the resulting drag.

NOMENCLATURE

D	= drag force
L	= lift force
C_D	= drag coefficient ($C_D = 2D/\rho V_\infty^2 S_F$)
C_L	= lift coefficient ($C_L = 2L/\rho V_\infty^2 S_F$)
ρ	= air density
V_∞	= free stream velocity
S_F	= reference area
M	= free stream Mach number
Re	= Reynolds number ($Re = V_\infty L_F/\nu$)
L_F	= length of fuselage
ν	= cinematic viscosity
α	= fuselage pitch angle
η	= Kolmogorov's length scale
L	= integral scale length
k	= turbulence kinetic energy
ε	= dissipation rate
P_A	= acoustic power per unit volume
p_s	= sound pressure
SPL	= Sound Pressure Level
ω_G	= angular frequency
ω_L	= rescaled integral scale frequency
a	= speed of sound

1. INTRODUCTION

Helicopter fuselage aerodynamics has been the subject of several investigations with some indicative results provided in references [1-3]. As reported in [4] there are substantial interactions between the flow structures formed at the rear part of the fuselage and these can even be affected by relatively small changes of the fuselage design. In general, the flow is characterised by large-scale coherent structures and smaller eddies that are typically modelled as turbulence. These flow structures are also responsible for some of the fuselage acoustic emission. Wavelengths that correspond to the mean-flow scales interact with the mean flow, and the larger-scale turbulent eddies, and mainly responsible for the energy cascade and the enhanced diffusivity of the flow. Most of the times, the flow at the rear fuselage is turbulent, and the flow structures generate strong broadband noise that adds to the overall acoustics of the aircraft.

For a conventional helicopter, there are two fundamental elements that contribute to the generation of near-field and far-field noise, the

main rotor and the tail rotor [5]. Engine and fuselage noise are typically of secondary significance. A helicopter main rotor generates primarily low frequency loading and broadband turbulence noise. Additional sources, including Blade Vortex Interaction (BVI) noise and High Speed Impulsive (HSI) noise, are dominant for specific operating regimes. BVI noise can be the most valuable contributor and has a strong component below and ahead of the rotor. Basic loading noise during hover is generally dominant in a conical region directed 30 to 40 degrees [5] downward from the rotor plane, while broadband noise radiates mostly out of the plane of the rotor. So for some operating conditions and for specific directions of sound propagation, broadband noise generated by all parts of helicopter (including fuselage) can be a significant contributor to the overall helicopter noise.

In a sense the study of broadband noise is driven by fixed wing flying vehicles. For example, as turbulent flow passes over the sharp trailing edge of an aerofoil, it generates strong broadband noise, which can be annoying to people [6]. Some elements of the helicopter fuselage may also have sharp edges, and can be the source of strong broadband noise.

The main goal of this paper is to look at the vortical structures generated by helicopter fuselage and its elements for fully turbulent flow using CFD solutions based on 3D steady Reynolds-Averaged Navier-Stokes (RANS) equations. In general, this approach allows for resolving low frequency (or large scale) vortical structures. However, CFD RANS solutions contain information about the distribution of turbulence in the flow. This information in combination with Proudman's approach [7] can be used for estimating the broadband fuselage noise.

For simulations an early model of the ANSAT helicopter produced by the JSC Kazan Helicopters are used. CFD computations and experiments were conducted for fuselage model with (without) skids and springs. Multiblock grids for CFD computations were constructed using the ANSYS ICEM software. The computational

domain was resolved using hexahedral grids and the 3D steady incompressible Reynolds-Averaged Navier-Stokes (RANS) equations. Fully turbulent calculations were performed using the $k-\omega$ model [8]. The computations were performed using the HMB solver of Liverpool University [9]. The results of the CFD modelling were compared to wind tunnel experimental data. Fuselage was tested at the low speed wind tunnel of KNRTU-KAI.

2. COMPARISON CFD DATA and WIND TUNNEL EXPERIMENT

The wind tunnel model fuselage (ANSAT-P of Fig. 1) was constructed using the same CAD file, used for CFD modelling. The aerodynamic performance of this model was considered in references [10-13], and was studied using the open test section (2.25 m diameter) closed circuit, low speed, wind tunnel T-1K that is equipped with a six-component Prandtl-type balance.



Fig. 1: ANSAT-P fuselage model in the test section of the T-1K tunnel.

The balance measurements were repeated eight-times to estimate random experiment errors (system errors, mounting of model errors, model construction errors, etc) and for plotting error bars.

The length of the ANSAT-P wind tunnel model (Figure 1) was $L_F=1.8$ m. The computational grid for this model (without skids and springs) contained 964 blocks and about 13.500.000 cells. The mesh topology and the

surface grid near the area of the exhausts are presented in Figure 2.

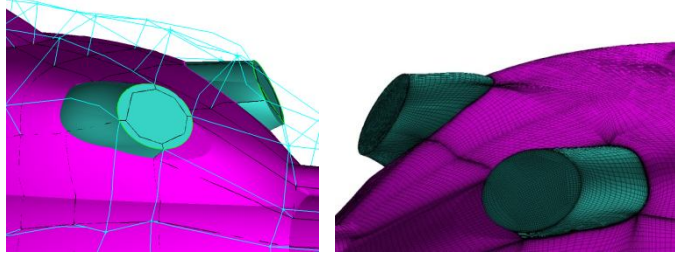
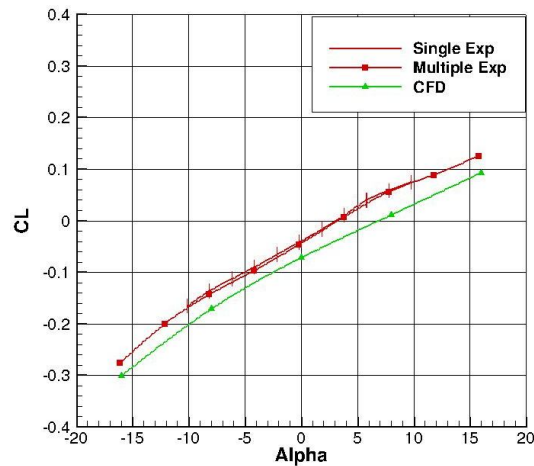
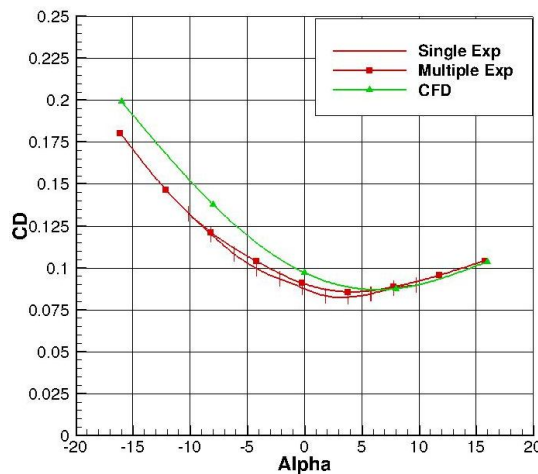


Fig. 2: Topology of blocks, and surface grid at the area of the engine exhausts

The conditions of the wind tunnel experiment and CFD modelling corresponded to the free stream Mach number and the Reynolds numbers were of 0.1 and $4.4 \cdot 10^6$, respectively.



a)



b)

Fig. 3: CFD and experimental lift (a) and drag (b) coefficients vs pitch angle

Figures 3, present the CFD results, compared with the wind tunnel experiment data. Experimental lift and drag coefficients are presented for single and multiple (octuple) experiments. From the figures, it follows that, in general, the CFD results for the ANSAT-P model are in good agreement with the experimental wind tunnel data, and that the overall aerodynamics of the fuselage is captured by the CFD computations.

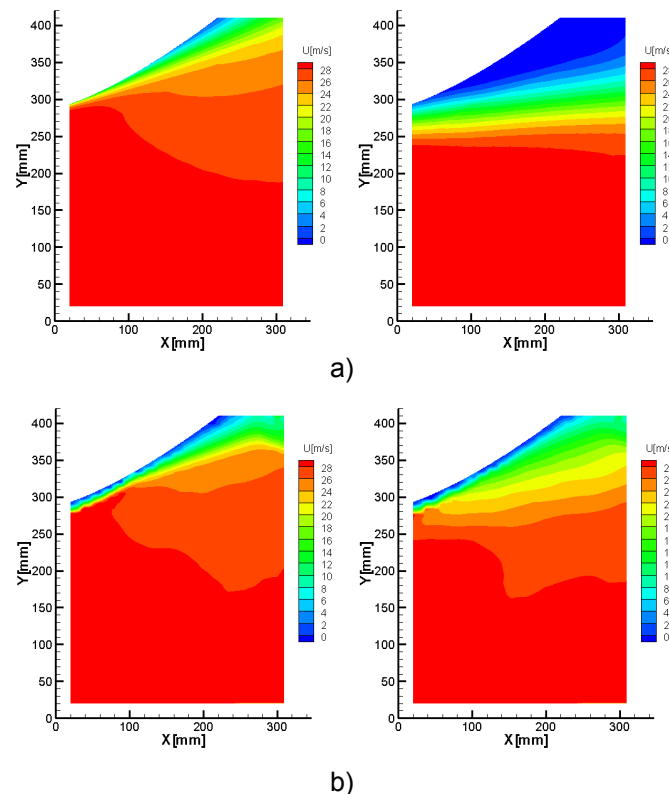


Fig. 4: CFD (a) and PIV (b) and symmetry plane velocity fields for $\alpha=0$ degree at rear part of fuselage (left figures) and fuselage with skids and springs (right figures)

Qualitative agreement of CFD and the experimental (PIV) velocity magnitude fields at the rear part of the fuselage model (without and with skids and springs) is shown in Fig. 4. For the isolated fuselage (without skids and springs) CFD and experimental PIV velocity fields have a minimal discrepancy. For the fuselage without skids and springs both approaches (CFD and experiment) revealed increasing of separation area; however the computed size of separation area is over predicted in comparison with

experiment. Perhaps reasons of discrepancy between CFD and experiment are limitations used for mathematical formulation of the current research. More accurate modelling of separated flow requires careful computations including fine grids, unsteady flow modelling, and advanced turbulence models.

3. TURBULENCE NOISE CHARACTERISTIC FREQUENCIES

One way to characterize a turbulent flow is by looking at the range of length and time scales. The N.-S. equations can be efficiently solved on a digital computer for essentially any physical flow. There are precisely features of turbulent flow that precludes use of DNS in most flow situations. Using RANS solutions it is only possible to resolve the low frequency turbulent structures to determine some basic performances of broadband noise.

Figure 5 shows a typical turbulence energy spectrum $E(k)$ for a high values of the Reynolds number (Re). The wavenumber k is the function of a sound wave length L_S : $k=2\pi/L_S$.

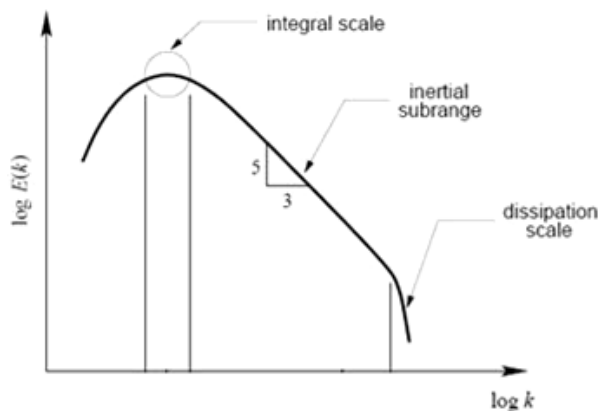


Fig. 5: Turbulence energy spectrum as a function of the wave number [14].

The turbulence energy spectrum can be divided into four areas (with some references combining the first two in one [see, for example [14]]):

- i) the large scale, based on the problem of domain geometry,
- ii) the integral scale, which is an $O(1)$ fraction (often taken to be ~ 0.2) of the large scale,

iii) the Taylor micro-scale or an intermediate scale, corresponding to Kolmogorov's inertial sub-range,

iv) the Kolmogorov (or "dissipation") scale which is the smallest of turbulence scales.

Kolmogorov's time, length scale and dissipation frequency can be estimated using:

$$\tau_k \sim (\nu/\varepsilon)^{1/2}, \quad \eta = (\nu^3/\varepsilon)^{1/4}, \quad f_d = 1/\tau_k. \quad (1)$$

Here ν is the kinematic viscosity, and ε is the dissipation rate [15]. We can compare the Kolmogorov's length scale η with the integral scale length L using ($L, \eta \in L_S$):

$$\eta \sim (\nu^3/|u'|^3 L)^{1/4}.$$

The symbol u' denotes a turbulent fluctuating component of velocity what is usually taken to be the square root of the turbulence kinetic energy (per unit mass)

$$|u'| = (2k)^{1/2}, \quad (2)$$

where k is turbulence kinetic energy. Hence

$$L \sim \eta^4 |u'|^3 / \nu^3.$$

Considering $|u'|$ as a velocity scale we can conclude that the integral scale frequency can be determined as

$$f_l \sim |u'|/L = \nu^3/(2\eta^4 k) = \varepsilon/(2k). \quad (3)$$

As $\varepsilon = \beta^* k \omega$ (ω is specific dissipation) we finally have

$$f_l \sim 0.5 \beta^* \omega. \quad (\beta^* = 0.09) \quad (4)$$

4. BROADBAND ISOTROPIC TURBULENCE NOISE (PROUDMAN'S FORMULA)

A simple approach to estimate acoustic emission of flying vehicle for turbulent flows, assumes that emitted noise does not have any distinct tones, and that the sound energy is continuously distributed over a broad range of frequencies. In this case the broadband noise power, can be estimated from RANS equations using the mean flow field, turbulent kinetic energy k and the dissipation rate ε . Unlike the direct method of simulation and the integral methods, Proudman's [7] approach does not require unsteady CFD solutions. This approach is based on Lighthill's acoustic analogy [16].

HMB has implemented Proudman's formula for acoustic power per unit of volume, generated by isotropic turbulence without mean flow.

According to the Proudman's formula the total radiated acoustic power per unit volume of turbulence is:

$$P_A = \alpha_\varepsilon \rho \varepsilon M_t^5, \quad (5)$$

where

$$M_t = (2k)^{1/2} / a.$$

Here a is the speed of sound, ρ is the air density. The re-scaled constant, α_ε , is set to 0.1 in HMB based on the reference [7].

The other estimation of the acoustic power per unit volume of turbulence was given by Lighthill [16]:

$$P_S \sim I L_{ref}^2. \quad (6)$$

Here L_{ref} is a reference length and I is the acoustic intensity which is the rate of energy transport across unit area for some characteristic velocity U , so that

$$I \sim \rho U^8 / a^5. \quad (7)$$

From the comparison of expressions (5) and (6), (7) we have that

$$I \sim P_S / L_{ref}^2 \sim P_A / L_{ref}^2.$$

Eventually we can write for the sound pressure:

$$p_S = (I \rho a)^{1/2} = (P_A \rho a / L_{ref}^2)^{1/2}. \quad (8)$$

5. VORTICAL STRUCTURES

Numerical modelling of flow structure and acoustic properties were considered for a fuselage configuration with skids added to the basic hull. The most complex case investigated included the fuselage layout with engine exhausts, tail boom, and skid assembly. The flow structures at the rear part of fuselage were found to be affected by the presence of the skids but also by the rather small tubular spring member connecting the port and starboard skid legs.

For an isolated fuselage body (without skids) it is known from literature, that two types of vertical structures can be found at the rear-facing separated flow region [5]: eddies that are located across the flow close to body-tail boom junction area, and vortex pairs located

symmetrically to the fuselage mid-plane and aligned with the free stream flow direction. Figure 6 presents the evolution of vortex pairs and eddies for different pitch angles.



(a)



(b)



(c)

Fig. 6: Evolution of vortexes pair (V-V) and eddy (E) for different pitch angles:
-8 degrees (a); 0 degrees (b); 8 degrees (c)

Iso-surfaces corresponding to velocity magnitude of $V=0.2V_\infty$ are used, where V_∞ is the free stream velocity. For areas without flow separation the iso-surfaces of $V=\text{constant}$, are close to the fuselage surface and the iso-surfaces geometry corresponds to fuselage geometry. In the separation zones, the iso-surfaces are detached to the fuselage surface and this allows the visualization of the zones.

Figure 6 suggests that the evolution of the vortex structure with the pitch angle is gradual. For negative value of pitch of -8 degrees the intensity of the vortex pair (V-V) is more than the intensity of eddy (E); and vice versa: for a positive value of pitch of 8 degrees the eddy (E) intensity is more than the intensity of vortex pair (V-V).

Figures 7 to 9 present some results of numerical modelling of the flow for different fuselage configurations at pitch angle of 0 degrees. Volume flow visualization is provided

by the stream-wise velocity iso-surfaces, and distribution of $\text{Vel}=V/V_\infty$.

One can see that there is a significant influence of the skid legs and springs on the separation area and the flow structures despite of the long distance between skid legs and the body-tail boom junction. The addition of the skid legs (Figure 8) did not change significantly the vortex structures in comparison with the clean fuselage. It leads, however, to stronger intensity of the vortex pair (V-V). However, adding a leaf-spring member to the fuselage with skids (Figure 9) leads to a completely new structure of the vortical flow. The extended separation zone and the more complex flow structure resulted in increased fuselage drag.

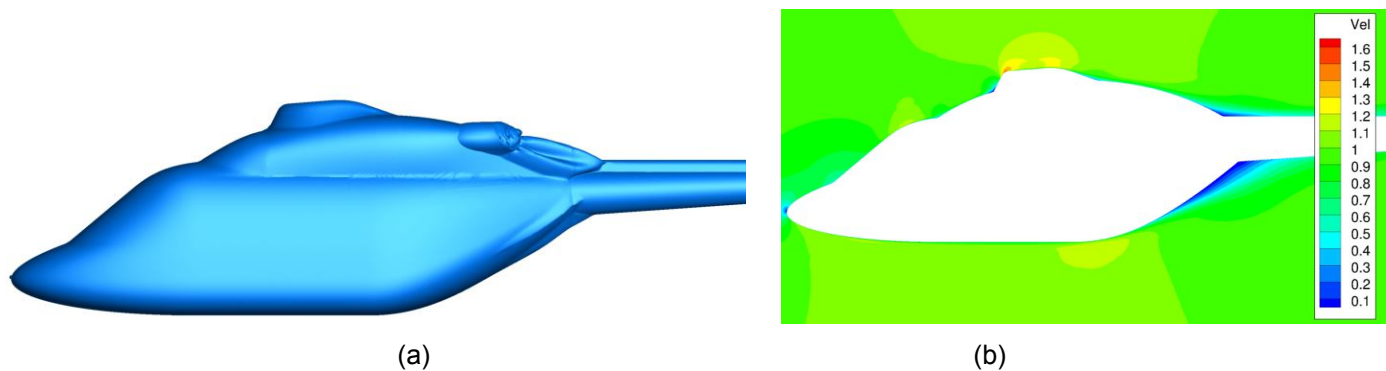


Fig. 7: Velocity iso-surface (a) and mid-ship velocity field (b) for fuselage without skids

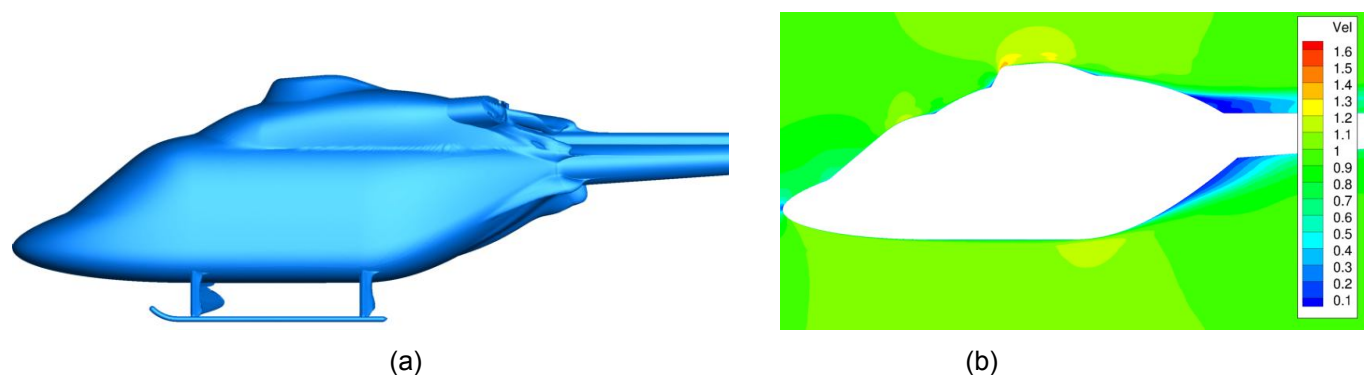


Fig. 8: Velocity iso-surface (a) and mid-ship velocity field (b) for fuselage with skids

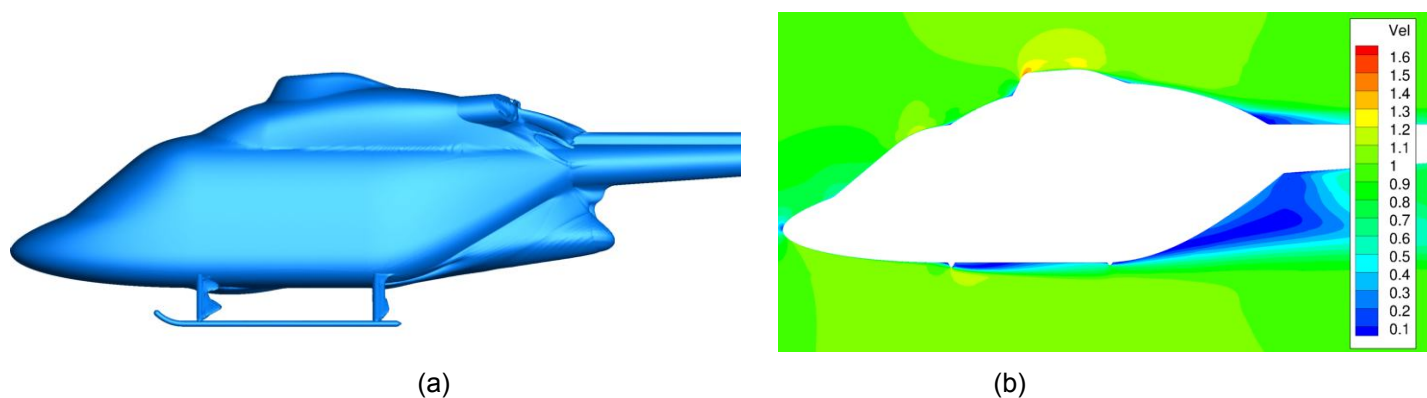


Fig. 9: Velocity iso-surface (a) and mid-ship velocity field (b) for fuselage with skids and springs

6. NOISE LEVEL AND FREQUENCY ANALYSIS

The Sound Pressure Level (SPL, dB) is evaluated according the formula

$$SPL = 20 \log_{10}(\rho_s / \rho_{ref})$$

Here ρ_s is the sound pressure, according to equation (8), and $\rho_{ref} = 2 \times 10^{-5}$ Pa. Figure 10 shows iso-surfaces of SPL values for the configurations with and without skids at 0 degrees of pitch angle.

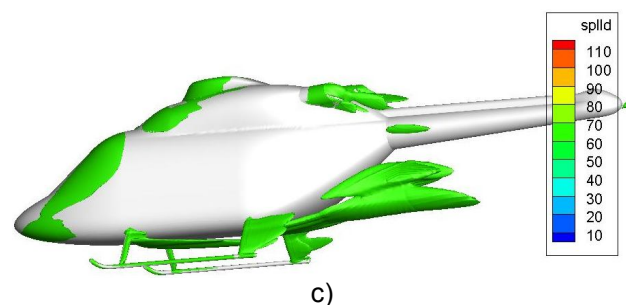
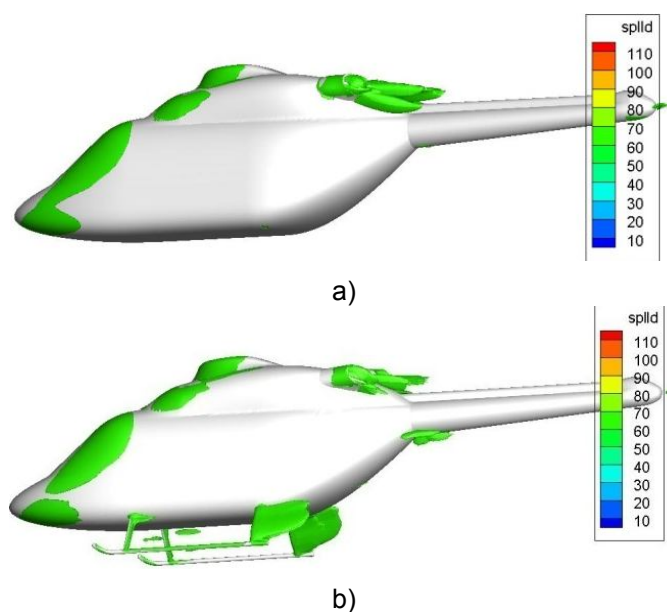


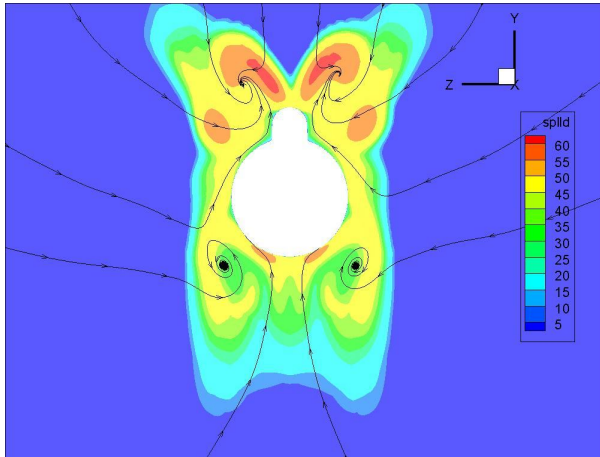
Fig. 10: Iso-surface of SPL for the fuselage (a), fuselage with skids (b) and with springs (c)

A relatively high level of SPL can be noted not only at the separation areas (behind the engine exhausts, skids and springs). The high level of SPL takes place also at the front part of helicopter fuselage where the boundary layer accelerates away from the front stagnation.

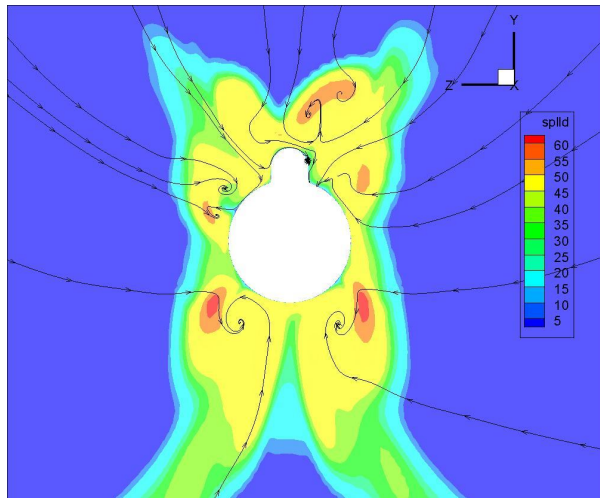
2D distribution of SPL and flow streamlines are given in a across the flow, located close to the junction of the tail boom and fuselage (Figure 11).

As expected, the addition to the fuselage of any new elements (skids and springs) increases the SPL value. According to equations (4), and (8), the values of SPL are influenced by the values of turbulence kinetic energy k . From equations (3), and (4) it follows that the k values also determine the spectrum of the acoustic emission.

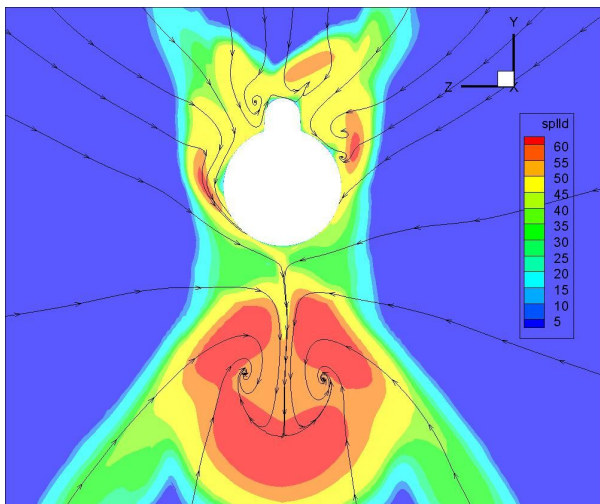




a)

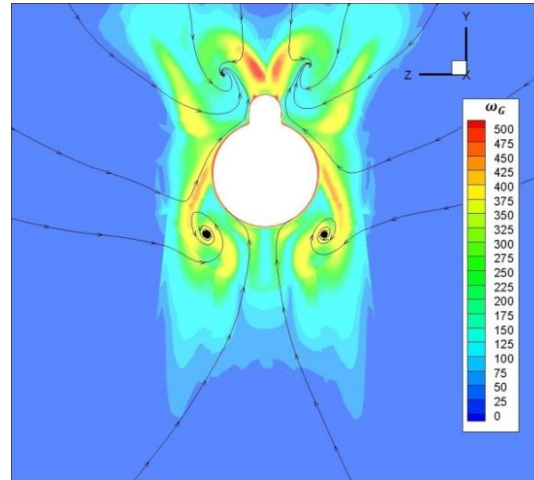


b)

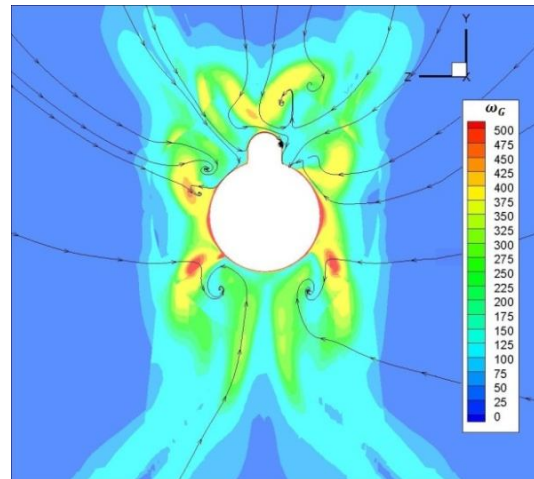


c)

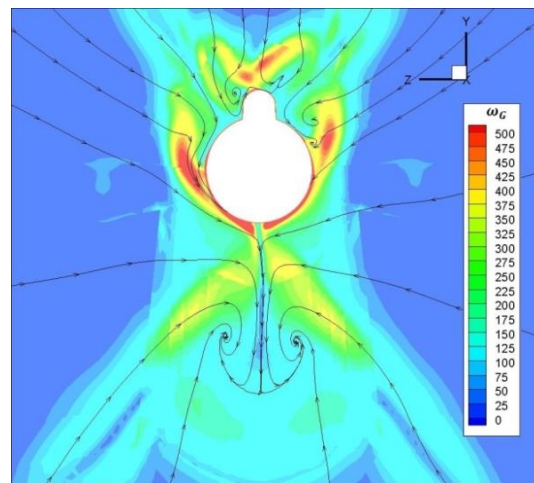
Fig. 11: 2D SPL distribution for the fuselage (a), fuselage with skids (b) and with springs at the 0 degree pitch angle



a)



b)



c)

Fig. 12: The angular frequency at the 0 degree pitch angle for the fuselage (a), fuselage with skids (b) and with springs (c)

Equation (4) can be written in the form

$$\omega_L \sim 0.5 \beta_L \beta^* \omega. \quad (9)$$

Here β_L is a dimensionless constant. The value of this constant can be determined from the analysis of distribution of the angular frequency ω_G (rad/s), according to :

$$\omega_G = (\omega_x + \omega_y + \omega_z)^{1/2}. \quad (10)$$

Here ω_x , ω_y , ω_z are components of the angular frequency vector.

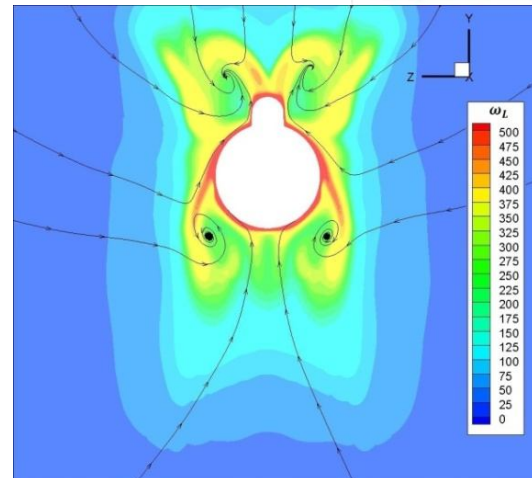
Figures 12, and 13 show the 2D distribution of the angular frequency ω_G and the rescaled integral scale frequency ω_L at the section, corresponding to the SPL distribution. The value of β_L coefficient in formula (9) was chosen of $0.6 \cdot 2\pi$ rad. In general images of ω_G and ω_L look similar with approximately the same range of values.

Therefore, equation (9) can be used to determine the angular frequency ω_G distribution (based on the specific dissipation ω distribution) and equation (10) can be used to determine the rescaled integral scale frequency ω_L distribution (based on the angular frequency ω_G distribution).

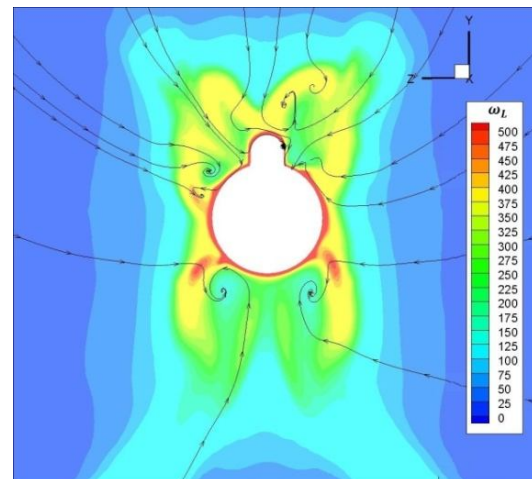
CONCLUSIONS AND FUTURE WORK

The structure and the acoustic properties of the flow around an idealized fuselage of the ANSAT helicopter were examined. The acoustic properties (broadband noise) of the flow and the frequency range of the vortical structures were estimated using Lighthill's acoustic analogy and the RANS equations, in terms of mean flow field, turbulent kinetic energy and the dissipation rate.

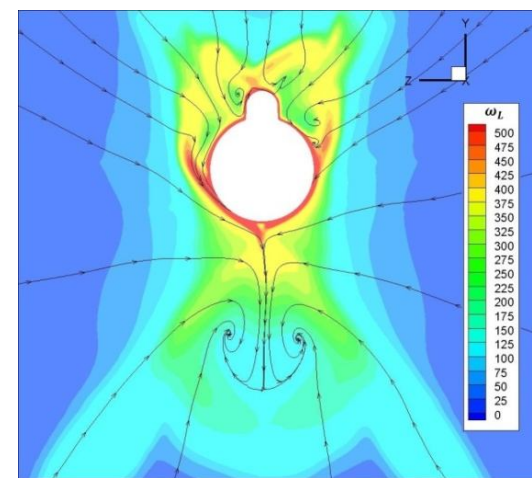
The agreement between the angular flow frequency and the rescaled integral length frequency was also investigated. In the future, the problem of the helicopter fuselage drag will be revisited using optimization theory in combination with CFD.



a)



b)



c)

Fig. 13: The integral scale frequency at the 0 degree pitch angle for the fuselage (a), fuselage with skirts (b) and with springs (c)

ACKNOWLEDGMENTS

This work is supported by the "Scientific projects in the framework of the state task realization" Grant.

Authors are grateful to T-1K wind tunnel group of KNRTU-KAI for the presented experimental data. The authors would like to acknowledge the Kazan Helicopter Plant for providing the initial fuselage shapes for this research.

Computations for this work have been conducted using clusters of KNRTU – KAI, Tatarstan Academy of Sciences and High Technology Technopark IT-park.

REFERENCES

1. Alascio A. D', Pahlke K. and Le Chuiton F. Application of a Structured and an Unstructured CFD method to the Fuselage Aerodynamics of the EC145 Helicopter. Prediction of the Time Averaged Influence of the Main Rotor., ECCOMAS, 24—28 July, 2004.
2. Le Chuiton F., D'Alascio A., Barakos G.N., Steijl R., Schwamborn D. and Ludeke H., EC145 Helicopter Fuselage - An Industrial Case, in W. Haase, M. Braza, A. Revell (Eds.), DESider - A European Effort on Hybrid RANS-LES Modeling, Notes on Numerical Fluid Mechanics and Multidisciplinary Design. Vol. 103, pp. 250-260, Springer Verlag, 2009.
3. Bridgeman J. O. and Lancaster G. T. Predicting Hub Drag on Realistic Geometries. Presented at the American Helicopter Society Aeromechanics Specialists Conference, San Francisco, California, January 20-22, 2010.
4. Seddon J. Basic Helicopter Aerodynamics, BSP professional Books, 1990, 136 pp.
5. Edwards B, Cox Ch. Revolutionary Concepts for Helicopter Noise Reduction — S.I.L.E.N.T. Program. NASA/CR-2002-211650, May 2002.
6. Arcondoulis E., Doolan C., Zander A. and Brooks L. An Experimental Investigation of Airfoil Tonal Noise Caused by an Acoustic Feedback Loop. Proceedings of Acoustics 2013 – Victor Harbor.
7. Proudman. The Generation of Noise by Isotropic Turbulence. Proc. Roy. Soc., A214:119, 1952.
8. Wilcox D. C. Reassessment of the Scale-determining Equation for Advanced Turbulence Models, AIAA J., Vol. 26, No. 11, pp. 1299–1310, 1988.
9. G. Barakos, R. Steijl, K. Badcock and A. Brocklehurst. Development of CFD Capability for Full Helicopter Engineering Analysis. 31st European Rotorcraft Forum, 13-15 September 2005, Florence, Italy, 2005.
10. Kusyumov A., Mikhailov S., Romanova E., Garipov A., Nikolaev E., Barakos G. Simulation of Flow around Isolated Helicopter Fuselage, EFM 2012 conference, Hradec Kralove, Czech Republic, 2012.
11. Batrakov A., Kusyumov A., Mikhailov S., Pakhov V., Sungatullin A., Zherekhov V., Barakos G. A Study in Helicopter Fuselage Drag. 39 European Rotorcraft Forum, Moscow, Russia, 2013.
12. Kusyumov A., Mikhailov S., Garipov A., Nikolaev E., Barakos G. Cfd Simulation of Fuselage Aerodynamics of the "ANSAT" Helicopter Prototype. Transactions on Control and Mechanical Systems. Vol. 1, No 7, pp. 318 – 324, 2012.
13. Batrakov A., Kusyumov A., Mikhailov S., Pakhov V., Sungatullin A., Zherekhov V., Barakos G. Helicopter Fuselage Drag Amelioration Using CFD and Experiments. Proceedings of the ASME 2013 International Mechanical Engineering Congress, San Diego, California, USA, 2013.
14. Chung T. J. Computational fluid dynamics, Cambridge University Press, 2010, 1034.
15. Terracol M., Sagaut P., Deck S. Multiscale and Multiresolution Approaches in Turbulence. 2nd Edition. World Scientific Publishing, 2013.
16. Lighthill M. J. On sound generated aerodynamically. I. General theory. Proc. Roy. Soc. London Ser. A 211 (1952), pp. 564–587. MR 13,879i. Zbl 049.259